Two-Phase Flow and Heat Transfer in Rectangular Micro-Channels

Weilin Qu
Graduate Research Assistant,
Student Mem. ASME
e-mail: quw@purdue.edu

Seok-Mann Yoon
Postdoctoral Research Associate
e-mail: smyoon@ecn.purdue.edu

Issam Mudawar
Professor and Director,
Fellow ASME
e-mail: mudawar@ecn.purdue.edu

Purdue University International Electronic Cooling Alliance (PUIECA),
Boiling and Two-Phase Flow Laboratory,
School of Mechanical Engineering,
Purdue University,
West Lafayette, IN 47907

Knowledge of flow pattern and flow pattern transitions is essential to the development of reliable predictive tools for pressure drop and heat transfer in two-phase micro-channel heat sinks. In the present study, experiments were conducted with adiabatic nitrogen-water two-phase flow in a rectangular micro-channel having a 0.406×2.032 mm² cross-section. Superficial velocities of nitrogen and water ranged from 0.08 to 81.92 m/s and 0.04 to 10.24 m/s, respectively. Flow patterns were first identified using high-speed video imaging, and still photos were then taken for representative patterns. Results reveal the dominant flow patterns are slug and annular, with bubbly flow occurring only occasionally; stratified and churn flow were never observed. A flow pattern map was constructed and compared with previous maps and predictions of flow pattern transition models. Features unique to two-phase micro-channel flow were identified and employed to validate key assumptions of an annular flow boiling model that was previously developed to predict pressure drop and heat transfer in two-phase micro-channel heat sinks. This earlier model was modified based on new findings from the adiabatic two-phase flow study. The modified model shows good agreement with experimental data for water-cooled heat sinks. [DOI: 10.1115/1.1756589]

Introduction

Two-phase micro-channel heat sinks have emerged in recent years as a prime contender for thermal management of next generation high-power-density commercial and defense electronics. These heat sinks feature flow boiling of liquid coolant through a series of parallel micro-channels with cross-sectional dimensions ranging from 10 to 1000 μm. The combination of small channel size and flow boiling offers many advantages such as low thermal resistance, small flow rate and coolant inventory, and stream-wise temperature uniformity.

Two-phase Heat Transfer in Micro-Channels. Because of these and other practical merits, two-phase micro-channel heat sinks have received considerable attention in recent years. An extensive review on the subject of boiling and two-phase flow in micro-channels and micro-channel structures has been provided by Ghiaasiaan and Abdel-Khalik [1]. Recent studies particularly concerned with transport phenomena in two-phase micro-channel heat sinks are summarized below.

Bowers and Mudawar [2–4] studied pressure drop and critical heat flux (CHF) of R-113 flow boiling in circular mini-channel (2.54 mm inner diameter) and micro-channel (510 μm inner diameter) heat sinks. A pressure drop model was developed to accurately predict experimental data. CHF values in excess of 200 W/cm^2 were obtained with both heat sinks. Peng and Wang [5] explored water flow boiling in 600×700 μm^2 rectangular micro-channels. Their results indicate channel size and geometry have a profound influence on flow boiling behavior. In particular, no apparent partial nucleate boiling existed for subcooled flow boiling, i.e., fully developed boiling was induced much earlier than in macro-channels. Jiang et al. [6] conducted visualization studies of water flow boiling in triangular micro-channels with nominal widths of 50 and 100 μm. Annular flow was the dominant flow pattern at moderate to high heat fluxes. The bubbly flow regime, common to macro flow boiling systems, was never observed. Zhang et al. [7] studied water flow boiling in rectangular micro-channels with hydraulic diameters from 25 to 60 μm and aspect ratios from 1.0 to 3.5. Nucleation and small bubble growth were observed inside the micro-channels at low heat fluxes, but annular flow became dominant at high heat fluxes. Hetsroni et al. [8] studied flow boiling of dielectric liquid Vertel XF in a micro-channel heat sink containing 21 parallel triangular micro-channels having a base dimension of 250 μm. The flow in the micro-channels alternated between single-phase liquid and elongated vapor bubbles. Qu and Mudawar experimentally studied pressure drop and heat transfer characteristics of water flow boiling in a rectangular micro-channel heat sink containing 231×713 μm^2 micro-channels [9–11]. Previous macro-channel models and empirical correlations were assessed and deemed unable to accurately predict pressure drop or heat transfer in micro-channel heat sinks. An annular flow model was developed to describe the heat transport characteristics of the heat sink, which showed excellent predictive capability.

These studies reveal that the flow boiling characteristics in micro-channel heat sinks deviate significantly from those in conventional macro-channels. Previous pressure drop and heat transfer models and correlations developed for macro-channel flow boiling fail to provide a satisfactory description of the flow in micro-channels. Overall, research in this area is still in its infancy and new research efforts are needed to develop a fundamental understanding as well as yield accurate predictive tools that are essential for heat sink design and optimization.

Knowledge of dominant two-phase flow patterns in micro-channels is key to developing accurate and physically sound predictive tools for heat sink design. As pointed out by Hosler [12], knowing which two-phase flow pattern prevails in a micro-channel is analogous to knowing whether a single-phase flow is turbulent or laminar. Unfortunately, interfacial interactions between the vapor and liquid phases during flow boiling in a micro-channel are often far too complex to permit accurate measurement or quantitative assessment of flow patterns. For a micro-channel heat sink, the situation is further complicated by the two-phase flow instability inherent to the multiple parallel channel arrangement. Flow patterns in micro-channel heat sinks can therefore only be determined in a qualitative manner. On the other hand, flow patterns of adiabatic gas-liquid two-phase flow in micro-

Contributed by the Electronic and Photonic Packaging Division for publication in the JOURNAL OF ELECTRONIC PACKAGING. Manuscript received December 2003. Associate Editor: B. Sammakia.

channels can be determined fairly accurately. An adiabatic micro-channel two-phase flow system may be used to simulate micro-channel flow boiling based on the assumption that if channel size and geometry as well as corresponding phase velocities are equal for the two systems, dominant flow patterns should also be the same.

Two-phase Flow Patterns in Micro-Channels. The present study was motivated by the lack of connection between studies on adiabatic two-phase flow in a single micro-channel and those concerning flow boiling in a multi-channel micro-channel heat sink. Such a connection is vital to developing a fundamental understanding of the transport behavior of micro-channel heat sinks, which can ultimately lead to a reliable and physically sound methodology for two-phase micro-channel heat sink design. In the present study, the connection is established by incorporating experimental results of adiabatic two-phase flow patterns in a rectangular micro-channel into an annular two-phase flow model that was previously developed by two of the present authors to describe water flow boiling in a rectangular micro-channel heat sink [10].

Adiabatic two-phase flow patterns in rectangular mini/micro-channels have been discussed in several recent studies. Mini-channels are channels with cross-sectional dimensions from 1 to a few millimeters, and micro-channels less than 1 mm. Wambsganss et al. [13] studied adiabatic air-water horizontal two-phase flow patterns in a rectangular mini-channel that was 3.18 mm deep and 19.05 mm wide. Four flow patterns (bubbly, plug, slug, and annular) were observed along the long (base) side of the channel. A comparison with previous flow pattern maps showed that, while these maps provide useful qualitative trends, they simply could not be relied upon for quantitative predictions. Ali and Kawaji [14] studied adiabatic air-water two-phase flow in a rectangular mini-channel (1.465 mm depth and 80 mm width) at four different orientations (vertical upflow and downflow, horizontal flow with long side or short side as base). Four flow patterns (bubbly, intermittent, rivulet, and annular) were observed for all orientations except horizontal flow with the short side as base. For this latter orientation, four flow patterns (bubbly, intermittent, plug, and stratified wavy) were identified. In general, transition to annular flow was observed at superficial air velocities much lower than those of macro-channels. Mishima et al. [15] studied adiabatic air-water vertical upflow in three rectangular mini-channels (1.0, 2.4, and 5.0 mm deep, and 40 mm wide). Four flow patterns (bubbly, slug, churn, and annular) were identified; churn flow was never observed in the 1.0 mm channel. Wilmarth and Ishii [16] studied adiabatic air-water two-phase flow in two rectangular mini-channels (1.0 and 2.0 mm depth with channel widths of 20 and 15 mm, respectively). The 1.0 mm channel was investigated in vertical upflow and the 2.0 mm in both vertical upflow and horizontal flow with the short side as base. Four flow patterns (bubbly, slug, churn-turbulent, annular) and three transition regions (cap-bubbly, elongated slug flow, churn-turbulent to annular) were observed for vertical upflow, while five flow patterns (stratified smooth, plug, slug, dispersed bubbly, wavy annular) and three transition regions (elongated plug, elongated slug, cap-bubbly) were identified for horizontal flow. Using a mixture of nitrogen and an ethanol-water liquid solution, Fujita et al. [17] studied adiabatic horizontal two-phase flow in five rectangular mini/micro-channels (0.2-2.0 mm in depth and 10 mm in width). Changing the ethanol concentration enabled them to vary surface tension of the liquid. Four flow patterns (plug, slug, streak, annular) were identified. Decreasing the liquid surface tension generally shifted the boundaries between flow patterns to lower superficial gas velocities. Xu et al. [18] studied adiabatic air-water vertical upflow in three rectangular mini/micro-channels (12 mm in width, 0.3, 0.6, and 1.0 mm in depth). Four flow patterns (bubbly, slug, churn, annular) and two transition regions (cap-bubbly, slug-churn) were identified in the 0.6 and 1.0 mm channels; only four flow patterns (cap-bubbly, slug-droplet, churn, annular-droplet) were observed in the 0.3 mm channel. With decreasing channel depth, the transition boundaries for bubbly-slug, slug-churn, and churn-annular flow all shifted to lower values of superficial gas velocity.

The above studies reveal many unique features of flow patterns in mini/micro-channels, including (1) the disappearance of certain flow patterns in mini/micro-channels, such as stratified and churn flow, and (2) the shift in flow pattern transition boundaries to lower superficial gas velocities. However, research in this area does not cover channel sizes and geometries found in micro-channel heat sinks. Most previous adiabatic two-phase mini/micro-channel studies concern rectangular channels with very small aspect ratio (ratio of depth to width), while practical micro-channel heat sinks mostly employ rectangular micro-channels with moderate aspect ratios of 0.2 to 1.0.

In this study, new experiments are conducted to explore flow patterns and flow pattern transitions of adiabatic nitrogen-water two-phase flow in a moderate aspect ratio rectangular micro-channel. Two-phase flow patterns in the micro-channel are first identified and discussed. Unique features are then employed to validate major approximations used in a previously developed annular flow model specifically tailored for flow boiling in micro-channel heat sinks. The earlier model is modified based on new findings from the adiabatic two-phase flow study. The predictions from the modified model are then compared with available experimental data for pressure drop and heat transfer coefficient in a water-cooled two-phase micro-channel heat sink.

Adiabatic Two-Phase Flow Patterns and Flow Pattern Transitions

Micro-channel Adiabatic Two-phase Flow Apparatus. Figure 1 shows a schematic of the flow loop that was constructed to supply the nitrogen-water two-phase mixture to the micro-channel test module. The water was circulated through the loop from a reservoir using a variable speed gear pump. The water was passed through a filter to remove any solid particles before entering one of five liquid rotameters for flow rate measurement. The nitrogen was supplied from a compressed nitrogen cylinder and its flow rate measured by one of five gas rotameters. Use of multiple rotameters for both fluids enabled testing broad flow rate ranges for both with accuracy better than 4%. After the flow rate measurement, both fluids entered a mixer to form a two-phase mixture. The mixture flowed through the micro-channel test module where the flow patterns were identified with the aid of both still photomicrography and high-speed video imaging. Exiting the test module, the two-phase mixture returned to the reservoir, where the nitrogen was released to the ambient through a vent. Several control valves were incorporated in the flow loop to aid in the flow control.

Figure 2(*a*) illustrates the construction of the test module that was composed of a base plate, a cover plate, a top (support) plate, and a pair of clamps. The three plates were fabricated from transparent acrylic to facilitate optical and visual access to the two-phase flow in the micro-channel. A rectangular micro-slot 0.406 mm deep, 2.032 mm wide, and 12 cm long was machined into the top surface of the base plate. The top plate, which was hollowed out in the middle, was pressed against the cover plate with the aid of the clamps to form the micro-channel. This arrangement enabled the use of a thin cover plate to bring the microscopic lens to within a very short distance from the flow, while providing sufficient mechanical pressure to compress an o-ring in the base plate and maintain a leak-proof assembly.

As shown in Fig. 2(*b*), the mixer consisted of a housing and a 40 μm porous tube. The nitrogen was bubbled into the water stream which was supplied through the annulus between the porous tube and housing.

The micro-channel test module was mounted horizontally with the cover plate facing upwards. Flow patterns were examined near the middle of the micro-channel to avoid inlet and outlet effects.

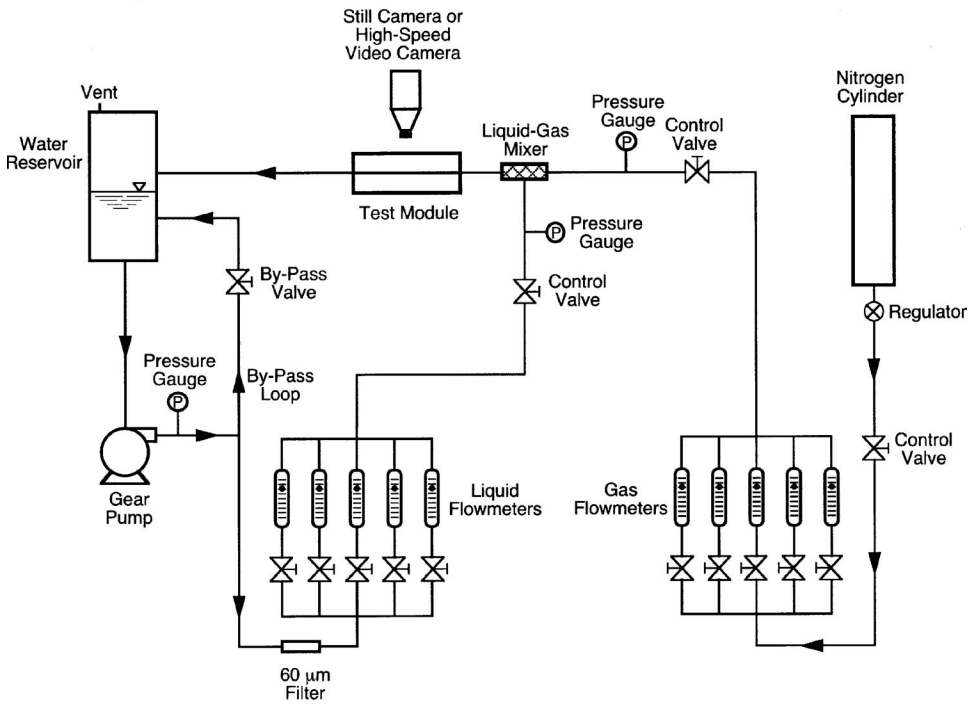

Fig. 1 Flow loop for adiabatic micro-channel two-phase flow study

The flow patterns were first identified with the aid of a high-speed video camera situated above the test module. Still photos were then taken for representative flow patterns using a Nikon camera that was fitted with a microscopic lens.

As indicated earlier, use of multiple rotameters for both fluids enabled testing over broad ranges of superficial velocities, 0.08-81.92 m/s for nitrogen and 0.04-10.24 m/s for water. The superficial velocities for nitrogen and water are defined as

$$j_g = \frac{Q_g}{A_{ch}} \tag{1}$$

and

$$j_f = \frac{Q_f}{A_{ch}}, \tag{2}$$

where A_{ch} is the micro-channel cross-sectional area, and Q_g and Q_f are the volume flow rates of nitrogen and water, respectively.

Flow Patterns. Figures 3(*a*) to 3(*e*) depict five distinct flow patterns that were identified for the adiabatic nitrogen-water two-phase micro-channel flow. The bubbly, stratified and churn flow patterns commonly encountered in macro-channels were never observed in the present study. On the left side of Figs. 3(*a*) to 3(*e*) are still photos of the dominant flow patterns, which are also illustrated schematically to the right of each photo. These flow patterns are based on the following characterization.

Slug flow–Illustrated in Fig. 3(*a*), this flow pattern features large nitrogen bubbles that are separated by water slugs. The nitrogen bubble width approaches that of the channel, while bubble length is several times the channel width. No water droplets are observed in the nitrogen bubble, nor are any nitrogen bubbles present in the water slugs.

Annular flow–As shown in Fig. 3(*b*), this flow pattern is characterized by a thin water film which flows along the channel wall with the nitrogen comprising the central core. Unlike annular macro-channel flow, the interface between the two phases is fairly smooth, and no droplets are entrained in the nitrogen core.

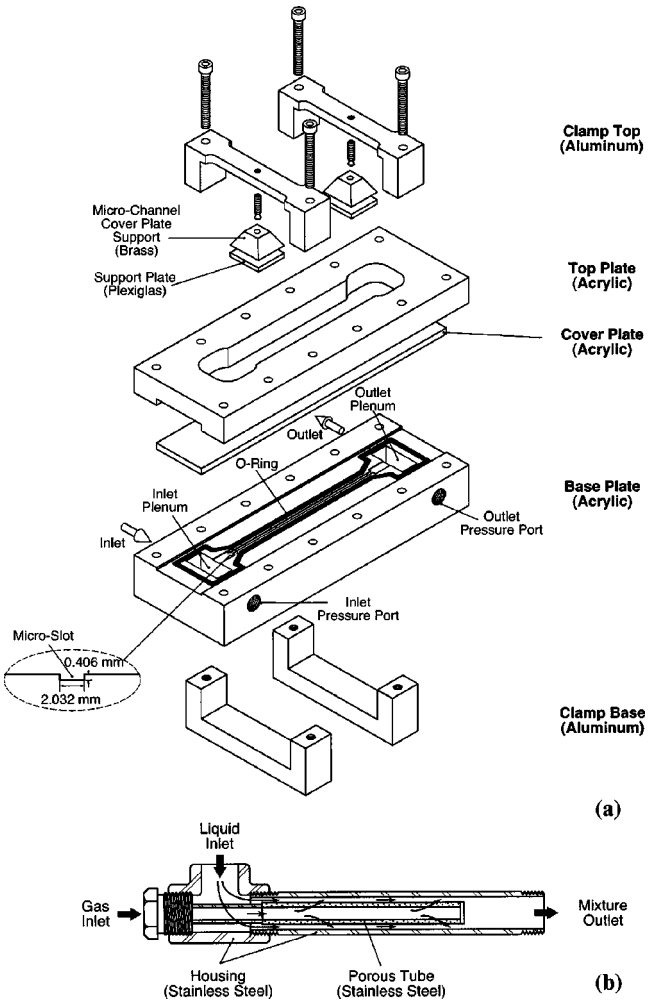

Fig. 2 (*a*) Test module for adiabatic micro-channel two-phase flow study, and (*b*) mixer construction

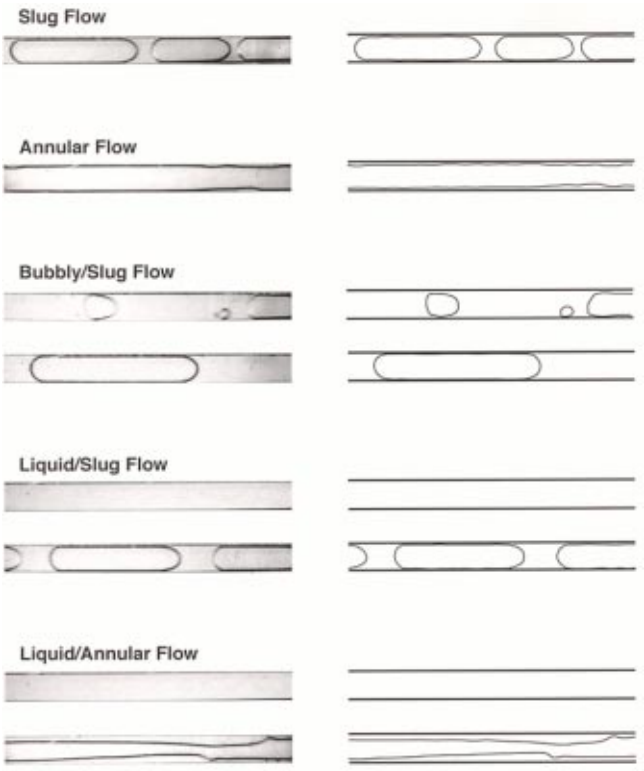

Fig. 3 Photographs and schematics of adiabatic micro-channel two-phase flow patterns: (*a*) slug flow, (*b*) annular flow, (*c*) bubble/slug flow, (*d*) liquid/slug flow, and (*e*) liquid/annular flow

Bubbly/slug flow–Shown in Fig. 3(*c*), this pattern is similar to slug flow except that nitrogen bubbles are observed in the liquid slugs. Viewed from above, these bubbles have a circular shape with a diameter smaller than the channel width.

Liquid/slug flow–Depicted in Fig. 3(*d*), this pattern is characterized by periodic oscillation between single-phase liquid flow and slug flow; the latter has the same features as those of the slug flow pattern.

Liquid/annular flow–As shown in Fig. 3(*e*), this flow pattern features periodic oscillation between single-phase liquid flow and annular flow.

Figure 4 depicts these flow patterns and the flow pattern transition boundaries in a flow pattern map utilizing the superficial velocities of nitrogen and water, j_g and j_f, respectively, as coordinates. At low values of j_f, the flow is slug or bubbly/slug for low j_g, but predominantly annular for high j_g. For high j_f, the flow transitions from liquid/slug to liquid/annular with increasing j_g.

Comparison With Prior Macro-channel Flow Pattern Maps and Transition Models. Mandhane et al. [19] developed one of the most popular flow pattern maps for horizontal adiabatic two-phase flow in macro-channels. Figure 5(*a*) shows significant discrepancy between their map and the present micro-channel data. Most notably, certain flow patterns in their map (stratified, wavy, dispersed) were never observed in the present study. Furthermore, the micro-channel data show an order of magnitude shift in j_g values corresponding to the transition to annular flow. These unique features of adiabatic two-phase micro-channel flow can be attributed to several factors, including strong effects of surface tension and negligible gravitational effects. In addition, low flow rates in micro-channels often produce laminar liquid and gas flows, a combination not commonly encountered in macro-channels.

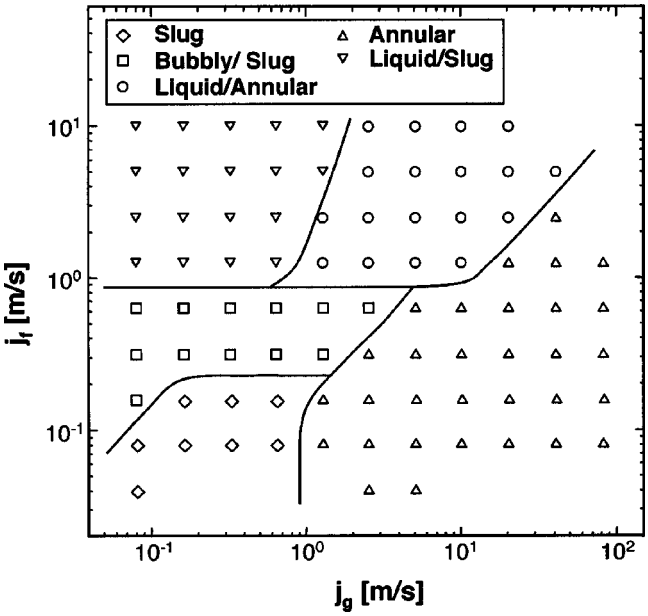

Fig. 4 Adiabatic micro-channel two-phase flow pattern map

Taitel and Duckler [20] and Weisman et al. [21] developed theoretical models to predict flow pattern transition boundaries for horizontal adiabatic two-phase flow. Key equations of these two models are summarized in Table 1. Figure 5(*b*) shows significant departure of the Taitel and Duckler models from the present data, especially at low j_g. However, predictions of the transition to annular flow are reasonably accurate. The predicted transition boundary between the stratified smooth and stratified wavy flow patterns is not plotted in Fig. 5(*b*) as the line falls outside the stratified region for the conditions of the present study.

Figure 5(*c*) shows poor agreement between the Weisman et al. models and present micro-channel data. The transition boundary between intermittent and dispersed flow has been excluded from this figure because it falls beyond the range of the present map.

Comparison With Prior Mini/Micro-channel Flow Pattern Maps. Figures 6(*a*)–(*f*) compare the present flow pattern map with those from previous studies on adiabatic two-phase flow in rectangular mini/micro-channels. The present map as well as all six previous maps show a shift in the transition to annular flow to j_g values significantly smaller than those of the Mandhane et al. map. Interestingly, this shift is greatest for the present map, which can be explained by the much smaller channel cross-sectional area utilized in the present study compared to the prior mini/micro-channel studies. There is also appreciable discrepancy in both flow patterns and transition boundaries among all mini/micro-channel studies. One possible reason for this discrepancy is the significant sensitivity of gas-liquid flow pattern to working fluid, channel size and geometry for mini/micro-channel flows, especially at low superficial velocities. A small change in channel size and geometry may significantly alter flow patterns and flow pattern transitions, which leads to the conclusion that a Mandhane et al. type universal flow pattern map may not be possible for micro-channel flow.

Due to the strong influences of both channel size and geometry on two-phase flow in micro-channels, the dimensionless parameters commonly employed in flow pattern transition models may not be adequate for micro-channel flow. Among others, the Confinement Number,

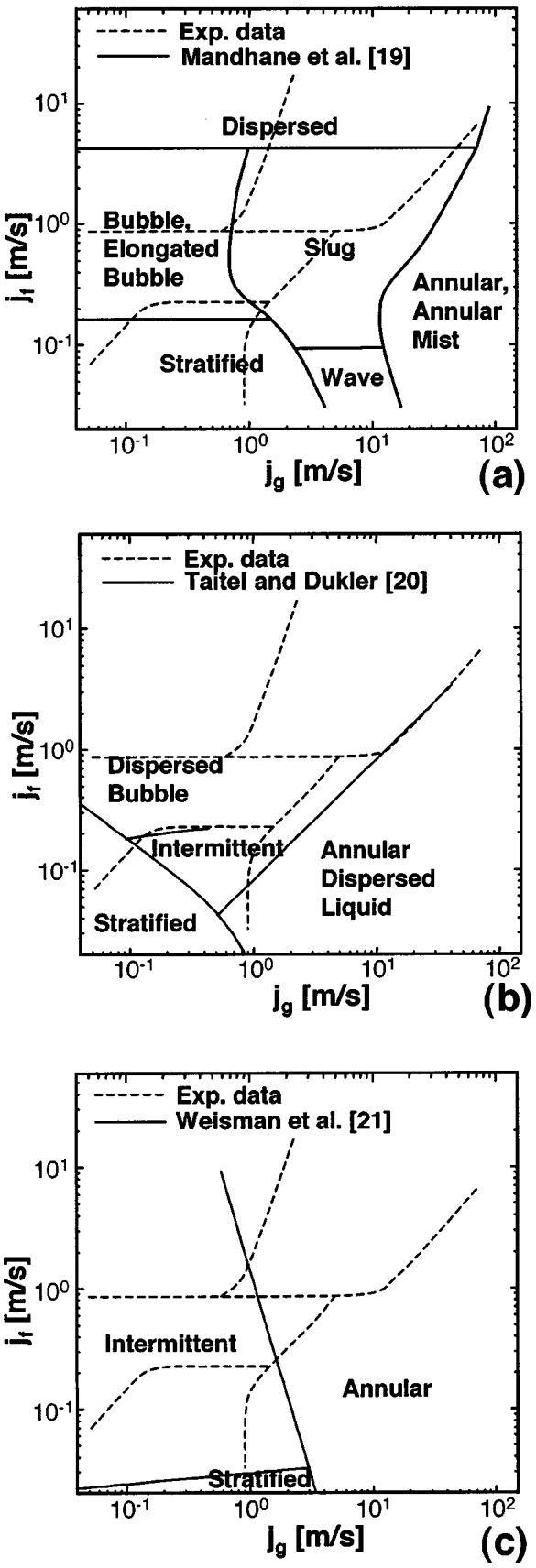

Fig. 5 Comparison of present flow pattern map with macro-channel maps and model predictions of (*a*) Mandhane et al. [19], (*b*) Taitel and Dukler [20], and (*c*) Weisman et al. [21]

$$Co = \frac{\sqrt{\dfrac{\sigma}{g(\rho_f - \rho_g)}}}{d_h}, \tag{3}$$

proposed by Cornwell and Kew [22] is often employed as a measure of channel size effects. The numerator in Eq. (3) is the Laplace constant, which is proportional to the wavelength of interfacial waves corresponding to the Taylor instability for horizontal two-phase flow. Suo and Griffith [23] suggested buoyancy effects become negligible for $Co \geqslant 3.3$. The confinement number for the present test is about 4.0, while those for the previous adiabatic mini/micro-channel studies span the range of 0.5 to 6.96 as indicated in Figs. 6(*a*)–(*f*). Large differences in Co between different studies suggest appreciable differences in channel wall effects, which might be one of the reasons behind the large deviations among different mini/micro-channel flow pattern maps.

In general, working fluids, channel size and channel geometry can alter the magnitude of several forces that are important to flow pattern development in mini/micro-channels. Aside from inertia, these include surface tension, gravity, and viscous forces. The confinement number Co discussed above is the ratio of surface tension force to gravity. Micro-channel two-phase flow is typically associated with large Co values, indicating a predominance of surface tension force over gravity. This may explain the disappearance of the stratified flow pattern in micro-channel flows.

Due to small channel size and small flow rates in micro-channels, the ratios of inertia to viscous force for each phase, which are represented by the following Reynolds numbers,

$$\mathrm{Re}_f = \frac{\rho_f j_f d_h}{\mu_f} \quad \text{and} \quad \mathrm{Re}_g = \frac{\rho_g j_g d_h}{\mu_g}, \tag{4}$$

fall mostly into the laminar range for both phases. The absence of strong turbulent mixing between the two phases may explain the disappearance of churn flow from some mini/micro-channel studies, as well as the lack of entrainment of small liquid droplets in the continuous gas core or small vapor bubbles in the liquid flow for adiabatic systems.

Overall, the great difficulty in generating a universal flow pattern map for adiabatic mini/micro-channel flows is a result of the need to maintain simultaneously the values of a large number of dimensionless parameters. This is a formidable task which, to the knowledge of the authors, has not been accomplished in any mini/micro-channel study. Such a map will require comprehensive study of the influences of Re_f and Re_g as well as each of the following dimensionless parameters:

$$We_f = \frac{\rho_f j_f^2 d_h}{\sigma} \quad \text{and} \quad We_g = \frac{\rho_g j_g^2 d_h}{\sigma}, \tag{5a}$$

$$Fr_f = \frac{j_f^2}{g d_h} \quad \text{and} \quad Fr_g = \frac{j_g^2}{g d_h}, \tag{5b}$$

$$Ca = \frac{\mu_f j_f}{\sigma}, \tag{5c}$$

and

$$S = \frac{j_g}{j_f}, \tag{5d}$$

where Weber numbers We_f and We_g are the ratios of inertia to surface tension, Froude numbers Fr_f and Fr_g inertia to gravity, Capillary number Ca liquid viscous force to surface tension, and S (slip ratio) vapor inertia to liquid inertia.

Table 1 Flow pattern transition models for horizontal adiabatic two-phase flow.

Reference	
	$X_{vv}\left(\frac{\overline{u_f}\overline{P_f}}{\overline{d_f}\overline{A_f}}\right)-\frac{\overline{u_g}}{\overline{d_g}}\left(\frac{\overline{P_g}}{\overline{A_g}}+\frac{\overline{P_i}}{\overline{A_f}}+\frac{\overline{P_i}}{\overline{A_g}}\right)=0$
	$X_{vv}=\frac{\mu_f j_f}{\mu_g j_g},\ \overline{A_f}=0.25[\pi-\cos^{-1}(2\overline{h_f}-1)$
	$+(2h_f-1)\sqrt{1-(2h_f-1)^2}]$
	$\overline{A_g}=0.25[\cos^{-1}(2\overline{h_f}-1)-(2\overline{h_f}-1)\sqrt{1-(2\overline{h_f}-1)^2}],$
	$\overline{P_f}=\pi-\cos^{-1}(2\overline{h_f}-1)$
	$\overline{P_g}=\cos^{-1}(2\overline{h_f}-1),\ \overline{P_i}=\sqrt{1-(2\overline{h_f}-1)^2},\ \overline{u_f}=\frac{A_{ch}}{d_h^2\overline{A_f}},$
	$\overline{u_g}=\frac{A_{ch}}{d_h^2\overline{A_g}}$
	$\overline{d_f}=\frac{4\overline{A_f}}{\overline{P_f}},\ \overline{d_g}=\frac{4\overline{A_g}}{\overline{P_g}+\overline{P_i}},\ \overline{h_f}=\frac{h_f}{d_h}$
Taitel and Dulder [20]	Transition between stratified and intermittent or annular-dispersed liquid patterns:
	$F^2\left[\frac{1}{(1-\overline{h_f})^2}\frac{\overline{u_g}\sqrt{1-(2\overline{h_f}-1)^2}}{\overline{A_g}}\right]\geq 1,\ F=\sqrt{\frac{\rho_g}{\rho_f-\rho_g}}\frac{j_g}{\sqrt{d_h g}}$
	Transition between intermittent and annular-dispersed liquid patterns:
	$\overline{h_f}=0.5$
	or $X_{vv}=1.93$
	Transition between stratified smooth and stratified wavy patterns:
	$K\geq\frac{20}{\sqrt{\overline{u_f}\overline{u_g}}},\ K=\sqrt{\frac{\rho_f\rho_g j_f j_g^2}{(\rho_f-\rho_g)d_h g\mu_f}}$
	Transition between intermittent and dispersed bubble patterns:
	$T^2\geq\frac{8\overline{A_g}\overline{d_f}}{\overline{P_i}\overline{u_f}}$
	$T=\sqrt{\frac{C_0\mu_f j_f}{(\rho_f-\rho_g)g d_h^2}},\ C_0=24(1-1.355\beta+1.947\beta^2-1.701\beta^3$
	$+0.956\beta^4-0.254\beta^5)$
Weisman et al. [21]	Transition between separated and intermittent patterns:
	$\frac{j_g}{\sqrt{d_h g}}=0.25\left(\frac{j_g}{j_f}\right)^{1.1}$
	Transition to annular pattern:
	$1.9\left(\frac{j_g}{j_f}\right)^{1/8}=\left(\frac{j_g\sqrt{\rho_g}}{[g(\rho_f-\rho_g)\sigma]^{1/4}}\right)^{0.2}\left(\frac{j_g^2}{d_h g}\right)^{0.18}$
	Transition to dispersed pattern:
	$\sqrt{\frac{C_0\mu_f j_f}{(\rho_f-\rho_g)g d_h^2}}\left[\frac{\sigma}{(\rho_f-\rho_g)d_h^2 g}\right]^{-0.25}=9.7$
	Transition between stratified and wavy patterns:
	$\left[\frac{\sigma}{(\rho_f-\rho_g)d_h^2 g}\right]^{0.2}\left(\frac{\rho_g j_g d_h}{\mu_g}\right)^{0.45}=8\left(\frac{j_g}{j_f}\right)^{0.16}$

Annular Two-Phase Flow Boiling Model

In this section, the experimental results of the above adiabatic micro-channel two-phase study are employed to validate an annular two-phase flow boiling model that was previously developed by two of the present authors to describe pressure drop and heat transfer characteristics of two-phase micro-channel heat sinks. The previous model is modified based on the new findings from the adiabatic study. Predictions of the modified model are compared with available pressure drop and heat transfer coefficient data obtained using a water-cooled two-phase micro-channel heat sink.

Model Construction. In a previous paper by two of the authors [10], a theoretical model based on the annular flow pattern was developed to describe the transport behavior of two-phase micro-channel heat sinks. Figure 7 illustrates the general features of the annular flow region. The vapor phase flows along the channel center as a continuous vapor core, and the liquid is comprised of two portions: one portion flows as a thin film along the channel wall, while the other is entrained in the vapor core as liquid droplets. The following key approximations are used to describe the flow structure adopted in the model development. The thickness of the annular liquid film is uniform along the channel circumfer-

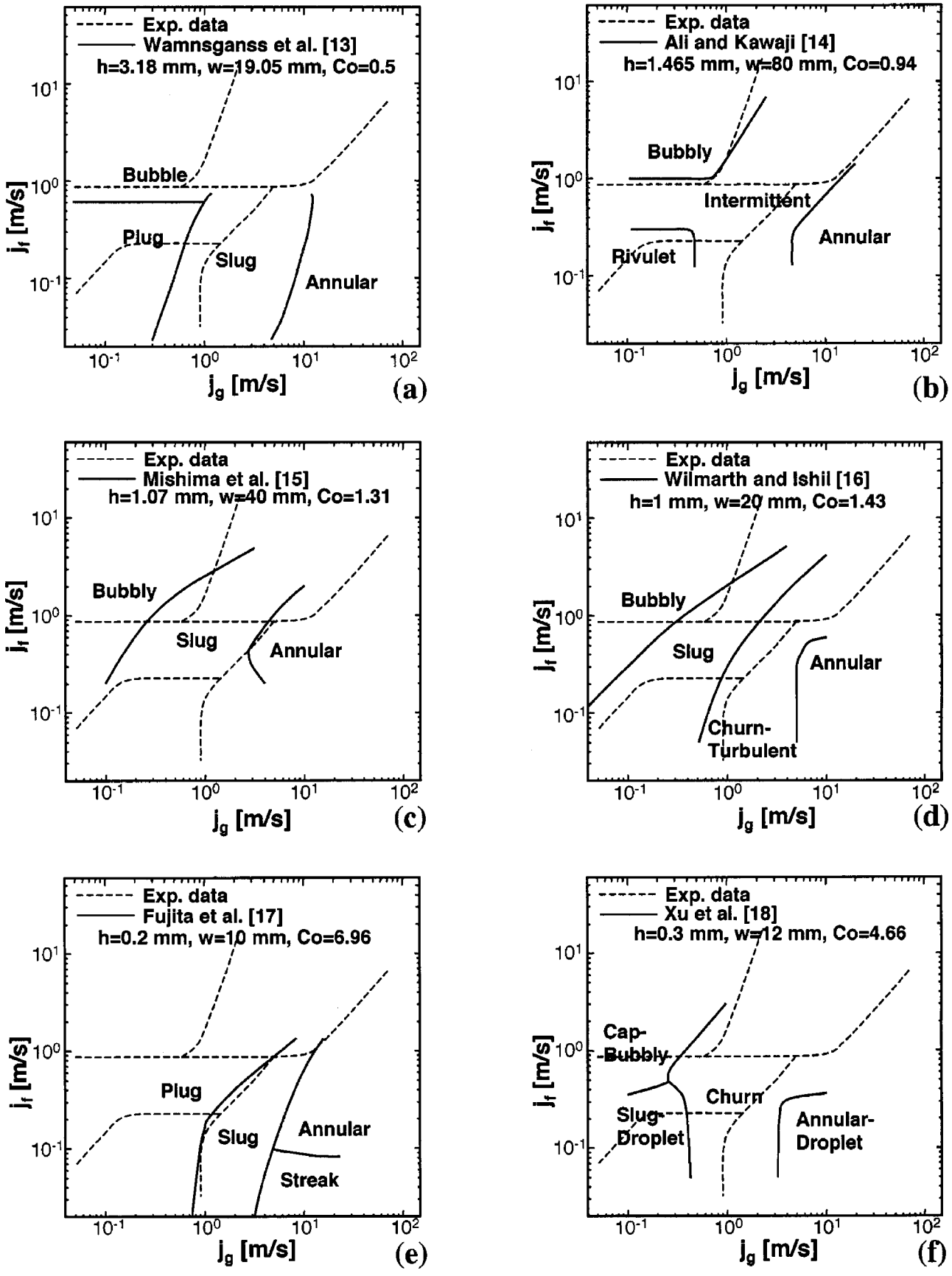

Fig. 6 Comparison of present flow pattern map with mini/micro-channel maps of (*a*) Wambsganss et al. [13], (*b*) Ali and Kawaji [14], (*c*) Mishima et al. [15], (*d*) Wilmarth and Ishii [16], (*e*) Fujita et al. [17], and (*f*) Xu et al. [18]

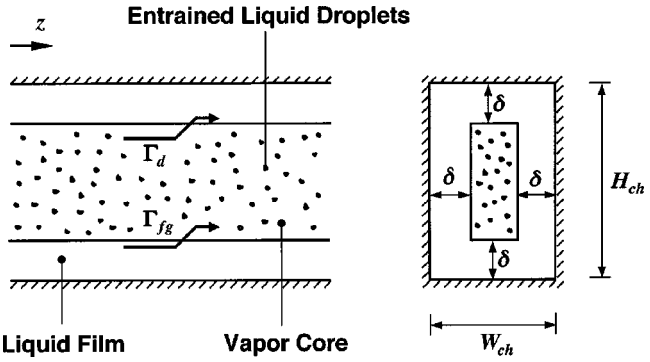

Fig. 7 Idealized annular flow region in two-phase microchannel heat sink

ence, and thin compared to the hydraulic diameter. Flows in both the liquid film and vapor core are laminar. The interface between liquid film and vapor core is smooth. Liquid droplets are assumed to be entrained into the vapor core entirely at the onset of annular flow pattern, and are gradually deposited onto the liquid film interface along the stream-wise direction.

The annular flow model is constructed by applying conservation equations to both the liquid film and vapor core. Key elements of the model are given below with details left in Ref. [10] for brevity.

Mass Conservation. Mass conservation in the liquid film and vapor core due to interfacial evaporation as well as droplet deposition requires that

$$\frac{dm_{Ff}}{dz} = -\Gamma_{fg} + \Gamma_d, \tag{6a}$$

$$\frac{dm_{Ef}}{dz} = -\Gamma_d, \tag{6b}$$

and

$$\frac{dm_g}{dz} = \Gamma_{fg}, \tag{6c}$$

where Γ_{fg} and Γ_d represent the rates of mass transfer by evaporation and deposition, respectively, per unit channel length. Details concerning the method for evaluating Γ_{fg} and Γ_d are given in Ref. [10].

Integrating Eqs. (6*a*) to (6*c*) leads to local values of m_{Ff}, m_{Ef}, and m_g. The following two boundary conditions are required to carry out the integration. The first is the location of the onset of annular flow, which is determined from [10]

$$X_{vv0} = \left(\frac{\mu_f}{\mu_g}\frac{1-x_0}{x_0}\frac{v_f}{v_g}\right)^{1/2} = 1.6. \tag{7}$$

The second is the initial liquid droplet mass flow rate m_{Ef0}, which can be evaluated using the relation [10]

$$m_{Ef0} = \left(0.951 - 0.15\sqrt{\frac{G^2 d_h v_f}{\sigma}}\right) m. \tag{8}$$

Momentum Conservation. Momentum conservation for the liquid film was analyzed using the control volume shown in Fig. 8(*a*). Momentum conservation requires that the sum of all forces acting on the liquid film control volume in the z direction equal

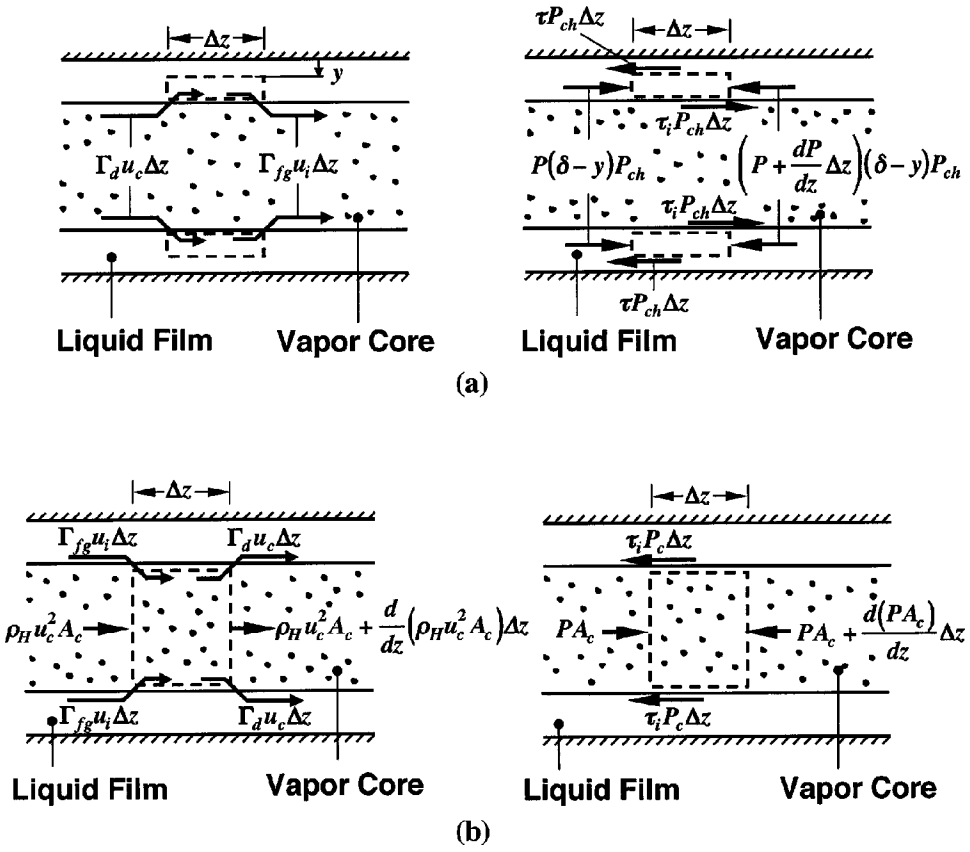

Fig. 8 Momentum conservation for control volumes encompassing (*a*) liquid film and (*b*) vapor core [10]

Table 2 Key equations in annular two-phase flow model.

Equation	
I	$\frac{dm_{Ff}}{dz}=-\Gamma_{fg}+\Gamma_d;\ \frac{dm_{Ef}}{dz}=-\Gamma_d;\ \frac{dm_g}{dz}=\Gamma_{fg}$ $\Gamma_{fg}=\frac{q''_{\text{eff}}W}{Nh_{fg}};\ \Gamma_d=DP_c$ $D=kC_{Ef};\ P_c=2[(W_{ch}-2\delta)+(H_{ch}-2\delta)]$ $C_{Ef}=\frac{m_{Ef}}{m_g v_g+m_{Ef}v_f};\ \frac{k}{j_g}=47.8Bo\left(\frac{C_{Ef}}{\rho_g}\right)^{-0.147};$ $Bo=\frac{q''_{\text{eff}}W}{N(W_{ch}+2H_{ch})Gh_{fg}};\ j_g=\frac{m_g}{\rho_g A_{ch}}$ B.C.: $\left(\frac{\mu_f}{\mu_g}\frac{1-x_0}{x_0}\frac{v_f}{v_g}\right)^{1/2}=1.93,$ $m_{Ef0}=\left(0.951-0.15\sqrt{\frac{G^2d_h v_f}{\sigma}}\right)m$
II	$m_{Ff}=\frac{P_{ch}\rho_f\delta^3}{3\mu_f}\left(-\frac{dp}{dz}\right)+\frac{P_{ch}\rho_f\delta^2}{2\mu_f}\tau_i-\frac{\rho_f\delta^2}{2\mu_f}(\Gamma_{fg}u_i-\Gamma_d u_c)$ $u_i=\frac{2m_{Ff}}{\rho_f(A_{ch}-A_c)};\ u_c=\frac{m_{Ef}+m_g}{\rho_c A_c};$ $A_c=(W_{ch}-2\delta)(H_{ch}-2\delta);\ \rho_c=\frac{m_g+m_{Ef}}{m_g v_g+m_{Ef}v_f}$
III	$\tau_i=\frac{1}{P_c}\left[A_c\left(-\frac{dP}{dz}\right)-P\frac{dA_c}{dz}\right]-\frac{1}{P_c}\frac{d}{dz}(\rho_c u_c^2 A_c)$ $+\frac{1}{P_c}(\Gamma_{fg}u_i-\Gamma_d u_c)$
IV	$\tau_i=f_i\left[\frac{1}{2}\rho_c(u_c-u_i)^2\right]-\frac{\Gamma_{fg}}{2P_c}(u_c-u_i)$ $f_i\,\text{Re}_C=24(1-1.355\beta_c+1.947\beta_c^2-1.701\beta_c^3+0.956\beta_c^4-0.254\beta_c^5)$ $\text{Re}_C=\frac{\rho_c(u_c-u_i)d_{h,c}}{\mu_g};\ \beta_c=\frac{W_{ch}-2\delta}{H_{ch}-2\delta};\ d_{h,c}=\frac{4A_c}{P_c}$

the net momentum in the same direction. This yields the following relation for shear stress across the laminar liquid film,

$$\tau=\mu_f\frac{du_f}{dy}=(\delta-y)\left(-\frac{dP}{dz}\right)+\tau_i-\frac{1}{P_{ch}}(\Gamma_{fg}u_i-\Gamma_d u_c). \quad (9)$$

The local velocity in the liquid film can be obtained by integrating Eq. (9), incorporating the non-slip condition of $u_f=0$ at $y=0$. Integrating the velocity profile across the film thickness yields

$$m_{Ff}=\frac{P_{ch}\rho_f\delta^3}{3\mu_f}\left(-\frac{dP}{dz}\right)+\frac{P_{ch}\rho_f\delta^2}{2\mu_f}\tau_i-\frac{\rho_f\delta^2}{2\mu_f}(\Gamma_{fg}u_i-\Gamma_d u_c). \quad (10)$$

Similarly, Momentum conservation for the vapor core was analyzed using the control volume shown in Fig. 8(*b*). Equating the net momentum in the z direction to the net force yields

$$\tau_i=\frac{1}{P_c}\left[A_c\left(-\frac{dP}{dz}\right)-P\frac{dA_c}{dz}\right]-\frac{1}{P_c}\frac{d}{dz}(\rho_H u_c^2 A_c)+\frac{1}{P_c}(\Gamma_{fg}u_i-\Gamma_d u_c). \quad (11)$$

Interfacial Shear Stress. The interfacial shear stress the between liquid film and vapor core is given by

$$\tau_i=f_i\left[\frac{1}{2}\rho_H(u_c-u_i)^2\right]-\frac{\Gamma_{fg}}{2P_c}(u_c-u_i). \quad (12)$$

Equation (12) assumes the liquid film and vapor core are both laminar. The second term to the right-hand side of Eq. (12) accounts for the effect of interfacial evaporation on shear stress.

The annular flow boiling model contains four primary parameters: m_{Ff}, δ, $-(dP/dz)$ and τ_i, which can be evaluated by solving the above equations [10]. All other parameters in the annular flow region, including pressure drop and heat transfer coefficient can be easily determined once the four primary parameters are obtained [10,11].

Assessment of Physical Basis of Annular Flow Boiling Model. The above annular flow boiling model was developed based on the assumption that annular flow is the dominant flow pattern in two-phase micro-channel heat sinks at moderate to high heat fluxes. This finding was obtained from flow visualization of a water-cooled two-phase micro-channel heat sink [9]. However, flow patterns in the micro-channel heat sink were only explored in a qualitative manner in the previous study [9] because of the technical difficulties previously discussed in this paper. In order to strengthen the physical basis of the model, key approximations

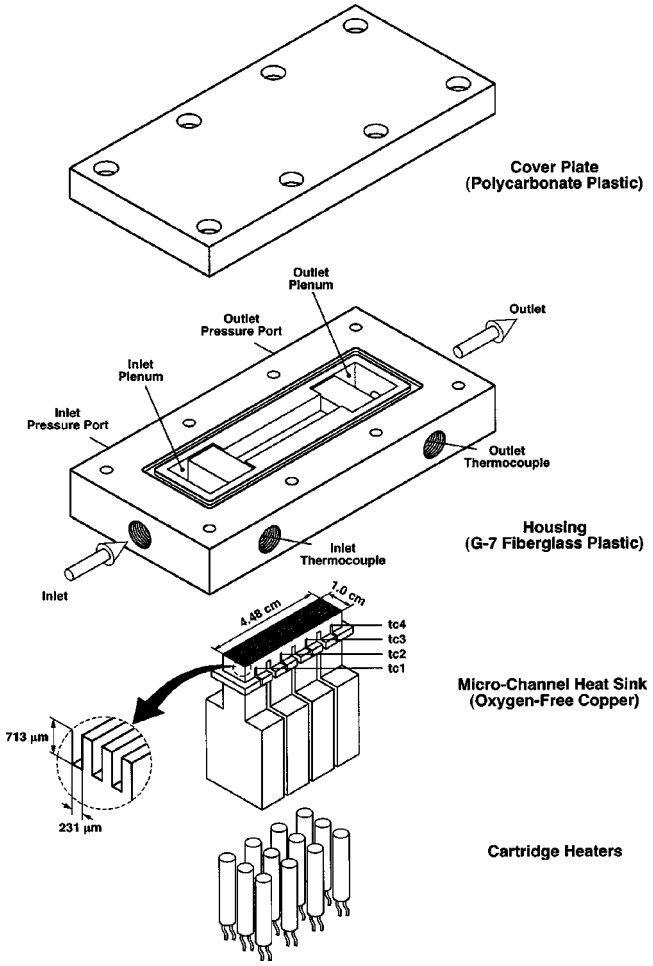

Fig. 9 Test module for two-phase micro-channel heat sink study

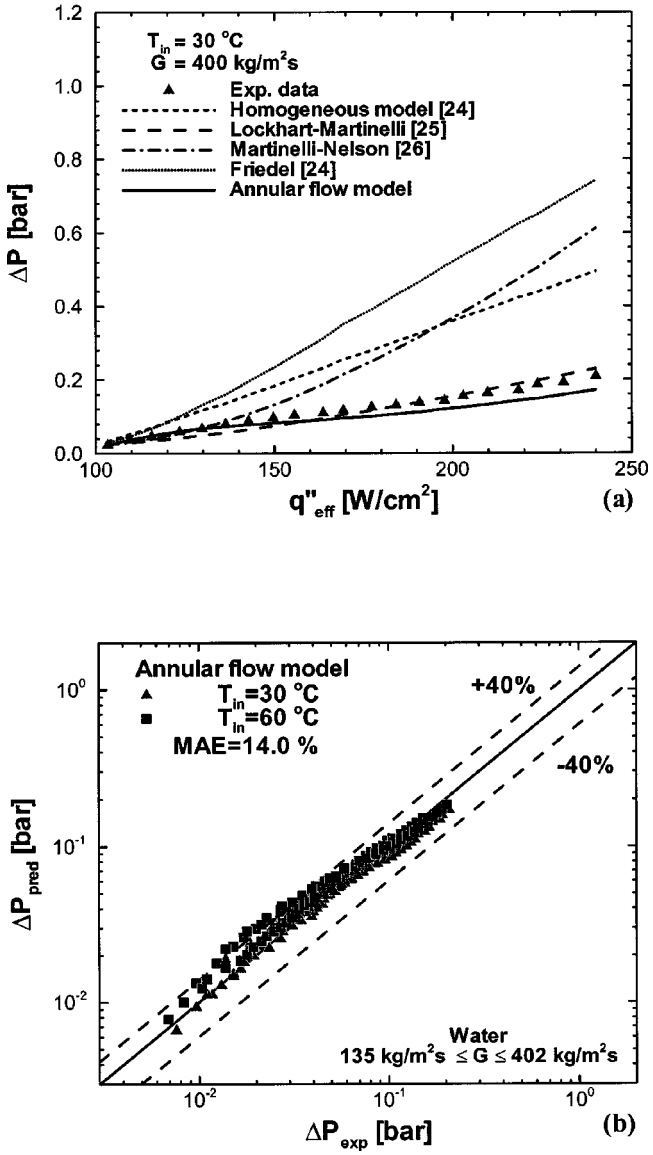

Fig. 10 (*a*) Comparison of predictions of annular flow model as well as popular macro-channel models and correlations with present pressure drop data for $T_{in}=30°C$ and $G=400$ kg/m^2 s. (*b*) Comparison of annular flow model predictions with all present pressure drop data

concerning the flow structure employed in the model are re-examined based on the new findings from the adiabatic study.

Unlike adiabatic two-phase flow, flow boiling produces appreciable axial variations in superficial liquid and vapor velocities, and corresponding axial changes in flow pattern. However, two-phase micro-channel heat sinks often utilize low coolant flow rates, which lead to low superficial liquid velocities. On the other hand, the superficial vapor velocity can increase very rapidly once flow boiling commences due to the intense vapor production. The net result is that broad ranges of superficial vapor and liquid velocities in two-phase micro-channel heat sink fall mostly into the lower right hand side of the present flow pattern map, which corresponds to the annular flow pattern. This is precisely the situation in the previous experimental study on the water-cooled two-phase micro-channel heat sink [9], where ranges of superficial vapor and liquid velocities were $j_g=0-116.0$ m/s and $j_f=0.12-0.42$ m/s, respectively. This shows annular flow is the dominant flow pattern in two-phase micro-channel heat sinks corresponding to moderate to high heat fluxes of practical interest, and the theoretical model based on the annular flow pattern is appropriate for describing flow boiling in water-cooled heat sinks.

A key assumption in the model development is that the interface between the liquid film and vapor core is smooth. This assumption was the basis for several key equations used in constructing the model (e.g., interfacial shear stress Eq. (12)). Additionally, it leads to another important approximation that the liquid droplets are entrained into the vapor core entirely at the onset of annular flow pattern development in the absence of any small wavelength disturbances along the film interface. The validity of this assumption can be justified by examining the annular flow pattern in Fig. 3. A fairly smooth interface exits between the liquid film and vapor core due to the strong influence of surface tension in micro-channels.

One should also be mindful of the limitations of the analogy between adiabatic two-phase flow in a micro-channel and flow boiling in a micro-channel heat sink. A key limitation is that the adiabatic system cannot simulate the liquid droplet behavior in the annular flow region. In fact, while the adiabatic study showed no liquid droplet entrainment in the gas core, flow visualization studies with the two-phase micro-channel heat sink revealed a large number of droplets were present in the vapor core [9].

As indicated in the previous section, the Taitel and Duckler [20] model provided fairly accurate prediction of the transition boundary to annular flow for adiabatic micro-channel flow. Their transition relation, which is based on the Martinelli parameter for laminar liquid-laminar vapor flow, is used here to determine the

vapor quality, x_0, corresponding to location of the onset of annular flow for micro-channel flow boiling. This leads to a criterion slightly different from the one used in the original model development [10], Eq. (7),

$$X_{vv0}=\left(\frac{\mu_f}{\mu_g}\frac{1-x_0}{x_0}\frac{v_f}{v_g}\right)^{1/2}=1.93. \quad (13)$$

In the following, Eq. (13) is used to replace Eq. (7) in the model development.

Comparison of Modified Model Predictions With Experimental Data. Key equations of the modified annular flow boiling model are summarized in Table 2. The modified model predictions are compared with experimental results for pressure drop and heat transfer obtained from a water-cooled two-phase micro-channel heat sink experimental facility. Detailed description of the experimental facility is available in Ref. [9]; only a brief overview is given here. As shown in Fig. 9, the test module consisted of a micro-channel heat sink, a housing, a cover plate, and twelve cartridge heaters. The top surface of the heat sink measured 1.0 cm wide and 4.48 cm long. Twenty-one rectangular 231-μm wide and 712-μm deep micro-slots were cut into the heat sink's top surface. Four thermocouples were embedded beneath the top surface to measure stream-wise temperature distribution along the heat sink; they are indicated in Fig. 9 as tc1 to tc4 from upstream to downstream. The bottom surface of the heat sink was bored to accommodate twelve cartridge heaters. The heat sink was inserted into the central hollowed portion of the housing. The housing contained deep and shallow plenums both upstream and downstream of the micro-channels to ensure even flow distribution. Two absolute pressure transducers were connected to the deep plenums via pressure taps to measure the inlet and outlet pressures, P_{in} and P_{out}. Also located in the deep plenums were two thermocouples to measure inlet and outlet temperatures, T_{in} and T_{out}. The micro-channels were formed by bolting the cover plate atop the housing. Water was used as working fluid. The accuracies of flow rate and pressure measurements were better than 4 and 3.5%, respectively, and thermocouple error was smaller than ± 0.3°C. Heat loss from the test module was estimated to be less than 4%. All heat fluxes presented in this study were therefore based on electrical power input, which was measured by a wattmeter having an accuracy of 0.5%. The operating conditions were as follows: inlet temperature of $T_{in}=30.0$ or 60.0°C, mass velocity of $G=134.9$ to 400.1 kg/m^2.s, and outlet pressure of $P_{out}=1.17$ bar. The input effective heat flux, q''_{eff}, based on the heat sink's top surface area, was adjusted to yield steady flow boiling in the micro-channels. The inlet and outlet pressures, P_{in} and P_{out}, inlet and outlet temperatures, T_{in} and T_{out}, and heat sink temperatures, T_{tc1} to T_{tc4} were all measured. From these, the pressure drop across the heat sink, ΔP, and heat transfer coefficient in the saturated region, h_{tp}, were evaluated. Detailed information concerning experimental data reduction can be found in refs. [9] and [11].

Figures 10(*a*) and 10(*b*) compare predicted pressure drop, ΔP_{pred}, and measured pressure drop, ΔP_{exp}. Figure 10(*a*) shows good agreement in both trend and magnitude between ΔP_{pred} and ΔP_{exp} for $T_{in}=30$°C and $G=400$ kg/m^2 s. Figure 10(*b*) shows the annular flow model provides good predictive capability when compared with the entire pressure drop database from the present study, evidenced by a mean absolute error (MAE) of 14.0%. Excepting the Lockhart-Martinelli correlation [25], Fig. 10(*a*) shows popular macro-channel pressure drop correlations [24,26] overpredict the present micro-channel pressure drop data by a large margin.

Figures 11(*a*) and 11(*b*) compare predictions of the annular flow model and measured saturated flow boiling heat transfer coefficient. Figure 11(*a*) compares the modified annular flow model predictions, $h_{tp,pred}$, and $h_{tp,\text{exp}}$ at the downstream thermocouple location as a function of thermodynamic equilibrium quality, x_e, for $T_{in}=30$°C and $G=400$ kg/m^2 s. Predictions based on popular flow boiling correlations [27–32] are also included for comparison. Figure 11(*a*) shows the present model accurately predicts both the trend and magnitude of h_{tp} while the previous correlations show poor predictions for both. The overall predictive capability of the annular flow model is illustrated in Fig. 11(*b*) for all the present saturated flow boiling micro-channel data. All data are shown located within a $\pm 40\%$ error band with a MAE of 12.2%.

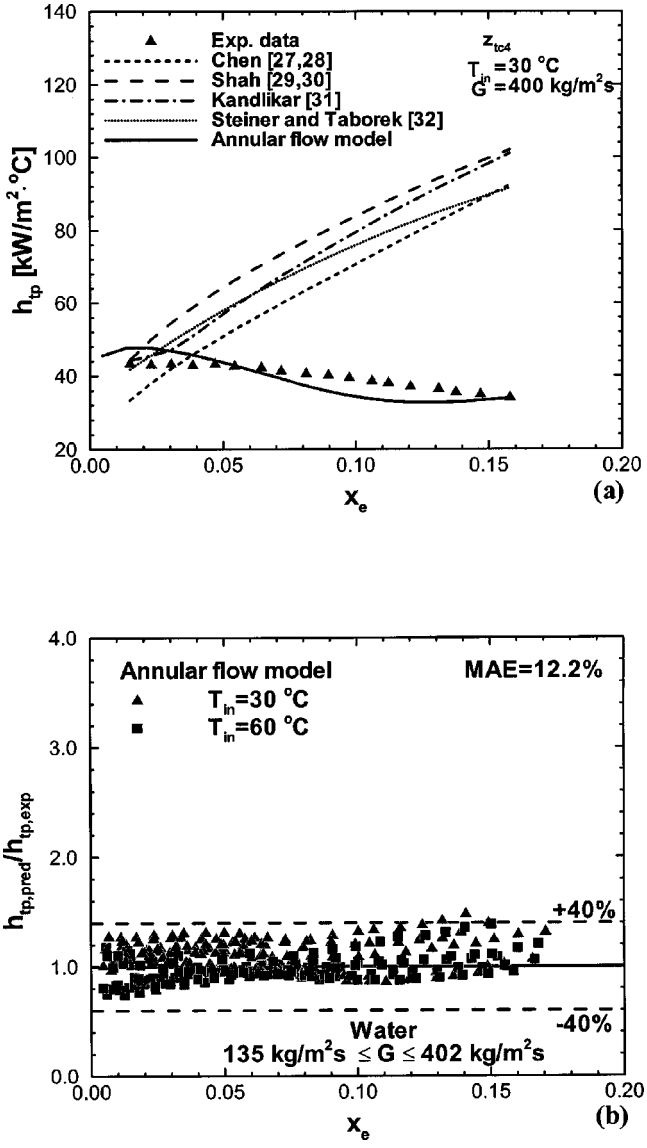

Fig. 11 (*a*) **Comparison of predictions of annular flow model as well as popular macro-channel correlations with present saturated flow boiling heat transfer coefficient data for $T_{in}=30$°C and $G=400$ kg/m^2 s.** (*b*) **Comparison of annular flow model predictions with all present saturated flow boiling heat transfer coefficient data**

Conclusions

Experiments were performed to study flow patterns and flow pattern transitions for adiabatic nitrogen-water two-phase flow in a rectangular micro-channel. Features unique to micro-channel two-phase flow were identified and incorporated into a theoretical model for flow boiling in micro-channel heat sinks. Key findings from the study are as follows:

1. Flow patterns in micro-channels deviate significantly from those in macro-channels. Slug and annular flow constitute

dominant flow patterns in micro-channels, and transition to annular flow occurs at much lower values of superficial gas velocity than macro-channels. There is also appreciable discrepancy in both flow patterns and transition boundaries among mini/micro-channel studies. Overall, this study shows it is difficult to generate a universal flow pattern map for adiabatic mini/micro-channel flows because of the need to maintain simultaneously values of a large number of dimensionless parameters.

2. Findings from the adiabatic two-phase flow patterns study validate key assumptions adopted in an annular flow boiling model that was previously developed to describe the pressure drop and heat transfer characteristics of two-phase micro-channel heat sinks. These assumptions include dominant annular flow pattern for moderate to high heat fluxes, smooth interface between the liquid film and vapor core, as well as droplet entrainment entirely at the onset of annular flow pattern development.
3. The annular flow boiling model is modified by incorporating new findings from the adiabatic two-phase flow study to predict the transition between annular flow and other flow patterns. Good agreement is achieved between the modified annular flow boiling model predictions and experimental data for both pressure drop and saturated flow boiling heat transfer coefficient in a water-cooled two-phase micro-channel heat sink.

Acknowledgment

The authors are grateful for the support of the Office of Basic Energy Sciences of the U.S. Department of Energy (Award No. DE-FG02-93ER14394 A7). Support for S.M. Yoon was provided by a postdoctoral fellowship program from the Korea Science and Engineering Foundation (KOSEF).

Nomenclature

A_c = cross-sectional area of vapor core
A_{ch} = channel cross-sectional area
$\overline{A_f}$ = dimensionless liquid cross-sectional area
$\overline{A_g}$ = dimensionless gas cross-sectional area
Bo = boiling number
C = liquid droplet concentration
Ca = capillary number
Co = confinement number
C_0 = constant in friction factor correlation
$\overline{d_f}$ = dimensionless liquid equivalent diameter
$\overline{d_g}$ = dimensionless gas equivalent diameter
d_h = hydraulic diameter of micro-channel
$d_{h,c}$ = hydraulic diameter of vapor core
D = deposition rate
F = constant in Taitel and Dukler's model
f_i = interfacial friction factor
Fr = froude number
g = gravitational constant
G = mass velocity
H_{ch} = height of micro-channel
h_f = enthalpy of saturated liquid; height of liquid phase
$\overline{h_f}$ = dimensionless liquid height
h_{fg} = latent heat of vaporization
h_{tp} = saturated two-phase heat transfer coefficient
j_f = superficial liquid velocity
j_g = superficial vapor/gas velocity
k = deposition mass transfer coefficient
K = constant in Taitel and Dukler's model
m = mass flow rate
m_{Ef} = liquid droplet mass flow rate
m_{Ff} = liquid film mass flow rate
m_g = vapor mass flow rate
MAE = mean absolute error
N = number of micro-channels in heat sink
P = pressure
P_c = vapor core perimeter
P_{ch} = channel perimeter
P_f = dimensionless channel perimeter in contact with liquid
$\overline{P_g}$ = dimensionless channel perimeter in contact with gas
$\overline{P_i}$ = dimensionless gas-liquid interfacial perimeter
q''_{eff} = heat flux based on heat sink top planform area
Q_f = liquid volume flow rate per channel
Q_g = gas volume flow rate per channel
Re = Reynolds number
Re_c = effective vapor core Reynolds number
S = slip ratio
T = temperature; constant in Taitel and Dukler's model
u_c = mean vapor core velocity
u_f = local velocity in liquid film
$\overline{u_f}$ = dimensionless liquid phase velocity
$\overline{u_g}$ = dimensionless gas phase velocity
u_i = interfacial velocity
v = specific volume
W = width of heat sink top planform area
W_{ch} = width of micro-channel
We = Weber number
x = vapor quality
x_e = thermodynamic equilibrium quality
X_{vv} = martinelli parameter based on laminar liquid–laminar vapor flow
y = distance perpendicular to channel wall
z = stream-wise distance

Greek Symbols

β = channel aspect ratio
β_c = aspect ratio of vapor core
Γ_d = deposition mass transfer rate per unit channel length
Γ_{fg} = evaporation mass transfer rate per unit channel length
δ = liquid film thickness
μ = viscosity
ρ = density
ρ_H = homogeneous density of vapor core
σ = surface tension
τ = local shear stress
τ_i = interfacial shear stress

Subscripts

0 = onset of annular flow
c = vapor core
E = liquid droplet
exp = experimental data
f = liquid
F = liquid film
g = vapor; gas
i = liquid film interface
in = inlet
out = outlet
$pred$ = predicted
tci = thermocouple ($i=1$ to 4)
tp = two-phase

References

[1] Ghiaasiaan, S. M., and Abdel-Khalik, S. I., 2001, "Two-Phase Flow in Micro-channels," Advances in Heat Transfer, Academic Press, New York, **34**, pp. 145–254.
[2] Bowers, M. B., and Mudawar, I., 1994, "High Flux Boiling in Low Flow Rate, Low Pressure Drop Mini-Channel and Micro-Channel Heat Sinks," Int. J. Heat Mass Transfer, **37**, pp. 321–332.
[3] Bowers, M. B., and Mudawar, I., 1994, "Two-Phase Electronic Cooling using Mini-Channel and Micro-Channel Heat Sinks: Part 1-Design Criteria and Heat Diffusion Constraints," ASME J. Electron. Packag., **116**, pp. 290–297.
[4] Bowers, M. B., and Mudawar, I., 1994, "Two-Phase Electronic Cooling using Mini-Channel and Micro-Channel Heat Sinks, Part 2: Flow Rate and Pressure

Drop Constraints,'' ASME J. Electron. Packag., **116**, pp. 298–305.
[5] Peng, X. F., and Wang, B. X., 1993, ''Forced Convection and Flow Boiling Heat Transfer for Liquid Flowing through Microchannels,'' Int. J. Heat Mass Transfer, **36**, pp. 3421–3427.
[6] Jiang, L., Wong, M., and Zohar, Y., 2001, ''Forced Convection Boiling in a Microchannel Heat Sink,'' J. Microelectromech. Syst., **10**, pp. 80–87.
[7] Zhang, L., Koo, J. M., Jiang, L., Banerjee, S. S., Ashegi, M., Goodson, K. E., Santiago, J. G., Kenny, T. W., 2000, ''Measurement and Modeling of Two-Phase Flow in Microchannels with Nearly-Constant Heat Flux Boundary Conditions,'' *Micro-Electro-Mechanical Systems (MEMS)-2000*, A. Lee et al., eds., ASME, MEMS-Vol. 2, pp. 129–135.
[8] Hetsroni, G., Mosyak, A., Segal, Z., and Ziskind, G., 2002, ''A Uniform Temperature Heat Sink for Cooling of Electronic Devices,'' Int. J. Heat Mass Transfer, **45**, pp. 3275–3286.
[9] Qu, W., and Mudawar, I., 2003, ''Flow Boiling Heat Transfer in Two-Phase Micro-Channel Heat Sinks-I. Experimental Investigation and Assessment of Correlation Methods,'' Int. J. Heat Mass Transfer, **46**, pp. 2755–2771.
[10] Qu, W., and Mudawar, I., 2003, ''Flow Boiling Heat Transfer in Two-Phase Micro-Channel Heat Sinks-II. Annular Two-Phase Flow Model,'' Int. J. Heat Mass Transfer, **46**, 2773–2784.
[11] Qu, W., and Mudawar, I., 2003, ''Measurement and Prediction of Pressure Drop in Two-Phase Micro-Channel Heat Sinks,'' Int. J. Heat Mass Transfer, **46**, pp. 2737–2753.
[12] Hosler, E. R., 1968, ''Flow patterns in High Pressure Two-Phase (Steam-Water) Flow with Heat Addition,'' *AIChE Symposium Series*, Vol. 64, pp. 54–66.
[13] Wambsganss, M. W., Jendrzejczyk, J. A., and France, D. M., 1991, ''Two-Phase Flow Patterns and Transition in a Small, Horizontal, Rectangular Channel,'' Int. J. Heat Mass Transfer, **17**, pp. 327–342.
[14] Ali, M. I., and Kawaji, M., 1991, ''The Effect of Flow Channel Orientation on Two-Phase Flow in a Narrow Passage between Flat Plates,'' *Proceedings of the 1991 ASME/JSME Thermal Engineering Joint Conference*, J. R. Lloyd, Y. Kurosaki, eds., ASME, New York, N.Y., Vol. 2, pp. 183–190.
[15] Mishima, K., Hibiki, T., and Nishihara, H., 1993, ''Some Characteristics of Gas-Liquid Flow in Narrow Rectangular Ducts,'' Int. J. Multiphase Flow, **19**, pp. 115–124.
[16] Wilmarth, T., and Ishii, M., 1994, ''Two-Phase Flow Regimes in Narrow Rectangular Vertical and Horizontal Channels,'' Int. J. Heat Mass Transfer, **37**, pp. 1749–1758.
[17] Fujita, H., Ohara, T., Hirota, M., and Furuta, H., 1995, ''Gas-Liquid Flows in Flat Channels with Small Channel Clearance,'' *Advances in Multiphase Flow*, A. Serizawa, T. Fukano, and J. Bataille, eds., Elsevier Science, New York, pp. 441–451.
[18] Xu, J. L., Cheng, P., and Zhao, T. S., 1999, ''Gas-Liquid Two-Phase Flow Regimes in Rectangular Channels with Mini/Micro Gaps,'' Int. J. Multiphase Flow, **25**, pp. 411–432.
[19] Mandhane, J. M., Gregory, G. A., and Aziz, K., 1974, ''A Flow Pattern Map for Gas-Liquid Flow in Horizontal Pips,'' Int. J. Multiphase Flow, **1**, pp. 537–553.
[20] Taitel, Y., and Dukler, A. E., 1976, ''A Model for Predicting Flow Regime Transitions in Horizontal and Near Horizontal Gas-Liquid Flow,'' AIChE J., **22**, pp. 47–55.
[21] Weisman, J., Duncan, D., Gibson, J., and Crawford, T., 1979, ''Effects of Fluid Properties and Pipe Diameter on Two-Phase Flow Patterns in Horizontal Line,'' Int. J. Multiphase Flow, **5**, pp. 437–462.
[22] Cornwell, K., and Kew, P. A., 1993, ''Boiling in Small Parallel Channels,'' *Energy Efficiency in Process Technology*, P. A. Pilavachi, ed, Elsevier Science, New York, pp. 624–640.
[23] Suo, M., and Griffith, P., 1964, ''Two-Phase Flow in Capillary Tubes,'' ASME J. Basic Eng., **86**, pp. 576–582.
[24] Collier, J. G., and Thome, J. R., 1994, *Convective Boiling and Condensation*, 3rd edition, Oxford University Press, Oxford.
[25] Lockhart, R. W., and Martinelli, R. C., 1949, ''Proposed Correlation of Data for Isothermal Two-Phase, Two-Component Flow in Pipes,'' Chem. Eng. Prog., **45**, pp. 39–48.
[26] Martinelli, R. C., and Nelson, D. B., 1948, ''Prediction of Pressure Drop during Forced-Circulation Boiling of Water,'' Trans. ASME, **70**, pp. 695–702.
[27] Chen, J. C., 1966, ''Correlation for Boiling Heat Transfer to Saturated Fluids in Convective Flow,'' I&EC Process Design and Development, **5**, pp. 322–329.
[28] Edelstein, S., Perez, A. J., and Chen, J. C., 1984, ''Analytic Representation of Convective Boiling Functions,'' AIChE J., **30**, pp. 840–841.
[29] Shah, M. M., 1976, ''A New Correlation for Heat Transfer during Boiling Flow Through Pipes,'' ASHRAE Trans., **82**, pp. 66–86.
[30] Shah, M. M., 1982, ''Chart Correlation for Saturated Boiling Heat Transfer: Equations and Further Study,'' ASHRAE Trans., **88**, pp. 185–196.
[31] Kandlikar, S. G., 1990, ''A General Correlation for Saturated Two-Phase Flow Boiling Heat Transfer Inside Horizontal and Vertical Tubes,'' ASME J. Heat Transfer, **112**, pp. 219–228.
[32] Steiner, D., and Taborek, J., 1992, ''Flow Boiling Heat Transfer in Vertical Tubes Correlated by an Asymptotic Model,'' Heat Transfer Engineering, **13**, pp. 43–69.